Smart Nanocarrier Based on PEGylated Hyaluronic Acid for Cancer Therapy

Ki Young Choi,[†,‡] Hong Yeol Yoon,[‡,§] Jong-Ho Kim,[⊥] Sang Mun Bae,[⊥] Rang-Woon Park,[⊥] Young Mo Kang,[⊥] In-San Kim,[⊥] Ick Chan Kwon,[‡] Kuiwon Choi,[‡] Seo Young Jeong,[†] Kwangmeyung Kim,[‡,*] and Jae Hyung Park[§,*]

[†]Department of Life and Nanopharmaceutical Sciences, Kyung Hee University, Seoul 130-701, Republic of Korea, [‡]Biomedical Research Institute, Korea Institute of Science and Technology, Seoul 136-791, Republic of Korea, [§]Department of Polymer Science and Engineering, Sungkyunkwan University, Suwon 440-746, Republic of Korea, and [⊥]Cell & Matrix Research Institute, School of Medicine, Kyungpook National University, Daegu 700-422, Republic of Korea

ABSTRACT Tumor targetability and site-specific drug release of therapeutic nanoparticles are key factors for effective cancer therapy. In this study, poly(ethylene glycol) (PEG)-conjugated hyaluronic acid nanoparticles (P-HA-NPs) were investigated as carriers for anticancer drugs including doxorubicin and camptothecin (CPT). P-HA-NPs were internalized into cancer cells (SCC7 and MDA-MB-231) *via* receptor-mediated endocytosis, but were rarely taken up by normal fibroblasts (NIH-3T3). During *in vitro* drug release tests, P-HA-NPs rapidly released drugs when incubated with cancer cells, extracts of tumor tissues, or the enzyme Hyal-1, which is abundant in the intracellular compartments of cancer cells. CPT-loaded P-HA-NPs (CPT-P-HA-NPs) showed dose-dependent cytotoxicity to cancer cells (MDA-MB-231, SCC7, and HCT 116) and significantly lower cytotoxicity against normal fibroblasts (NIH-3T3) than free CPT. Unexpectedly, high concentrations of CPT-P-HA-NPs demonstrated greater cytotoxicity to cancer cells than free CPT. An *in vivo* biodistribution study indicated that P-HA-NPs selectively accumulated into tumor sites after systemic administration into tumor-bearing mice, primarily due to prolonged circulation in the blood and binding to a receptor (CD44) that was overexpressed on the cancer cells. In addition, when CPT-P-HA-NPs were systemically administrated into tumor-bearing mice, we saw no significant increases in tumor size for at least 35 days, implying high antitumor activity. Overall, P-HA-NPs showed promising potential as a drug carrier for cancer therapy.

KEYWORDS: hyaluronic acid · nanoparticle · Hyal-1 · camptothecin · drug release · tumor targeting

Recent research for cancer therapy has centered on the development of polymeric nanoparticles that are capable of targeting tumors.[1−4] Following systemic administration into tumor-bearing mice, polymeric nanoparticles selectively accumulate into the tumor site either by the enhanced permeation and retention (EPR) effect[5,6] or by specific binding to receptors that are overexpressed on cancer cells.[7−9] These nanoparticles facilitate delivery of anticancer drugs into tumor tissues at high concentrations, leading to effective eradication of malignancy. To facilitate selective delivery of anticancer drugs to tumor tissue, numerous nanoparticles with sophisticated structures have been designed to exhibit physicochemical changes responding to extracellular or intracellular stimuli such as pH,[10−14] reductive potential,[15,16] and enzymes.[1,17,18] It is generally accepted that maximum therapeutic efficacy can be achieved by using nanoparticles that can effectively reach the tumor site, be internalized by endocytosis *via* binding to a specific receptor on the tumor cell, and then quickly release the drug at the intracellular level.

Hyaluronic acid (HA), also called hyaluronan, is an anionic, naturally occurring polysaccharide that is a major extracellular constituent of connective tissues.[19,20] Because HA can bind to CD44, a receptor that is overexpressed on various tumor cells, recent studies have focused on pharmaceutical applications of HA for the development of anticancer therapeutics.[21−23] HA also readily degrades into low molecular weight fragments in vertebrates due to hyaluronidases (Hyals),[24] enzymes whose levels are known to increase in various malignant tumors including prostate,[25,26] bladder,[27,28] head and neck,[29] colorectal,[30] brain,[31] and metastatic breast cancers.[32,33] Owing to high levels of Hyals, HA turnover occurs more rapidly in malignant tissues,[20,24,34] and low molecular weight HA fragments are found in much greater amounts at tumor sites than in normal tissues.[35]

Of various Hyals controlling HA catabolism in somatic tissues, Hyal-1 is the major enzyme found in tumor tissues.[20] Although Hyal-2 initiates extracellular degradation of HA,[36] HA turnover occurs mainly within cells due to Hyal-1.[34,36] Accordingly, receptor-mediated internalization of HA is the crucial step for HA catabolism. HA first binds to the receptor (CD44) on the surface of the cancer cell and is then cleaved into units up to 50 saccharides long by Hyal-2 on the cell surface, forming caveolae. As the caveolae become endosomes and finally fuse with lysosomes, the HA fragments are further degraded into tetrasaccharides by Hyal-1.[20,34,37]

* Address correspondence to jhpark1@skku.edu; kim@kist.re.kr.

Received for review June 6, 2011 and accepted October 3, 2011.

Published online October 03, 2011
10.1021/nn202070n

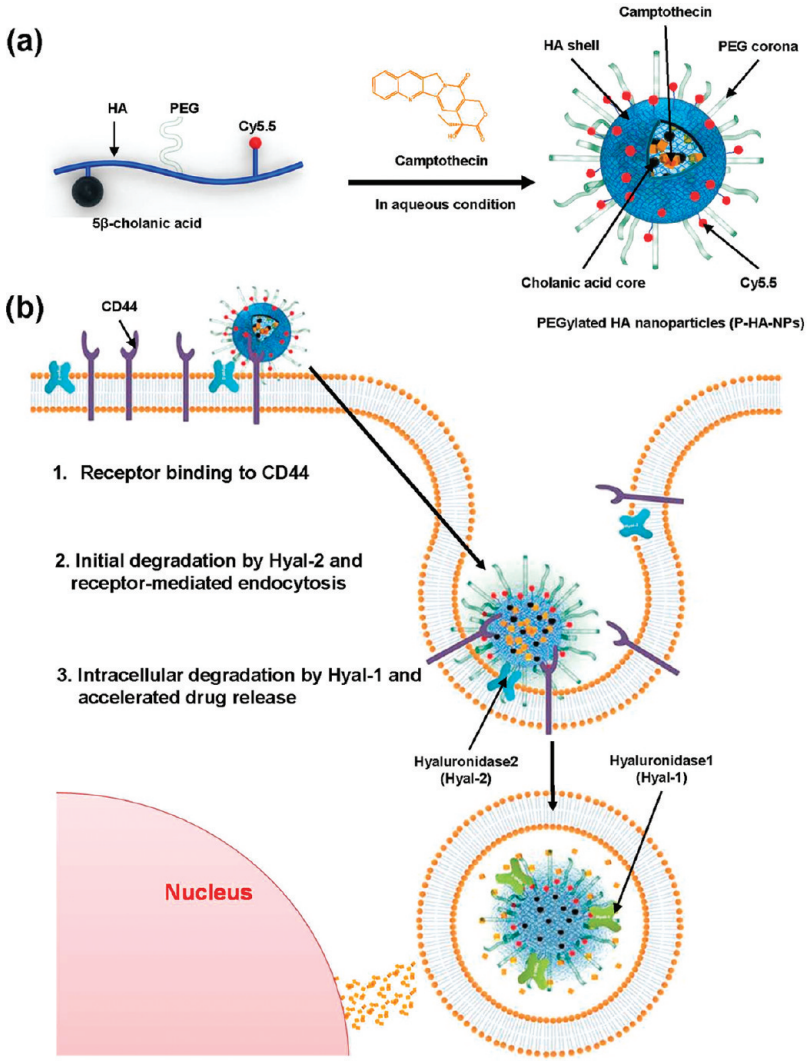

Figure 1. Schematic illustrations of (a) the formation of drug-loaded P-HA-NPs and (b) hypothetical cellular uptake pathways and subcellular drug release behaviors.

This unique degradation pathway for HA may allow its use as a carrier for selective drug delivery to intracellular compartments. It should be emphasized that the potential of self-assembled HA nanoparticles (HA-NPs) for use as drug carriers has not yet been reported.

Our group has developed HA-NPs for cancer therapy that can be self-assembled into nanosized particles in a physiological solution.[9,38,39] When bare HA-NPs are administered into tumor-bearing mice, they selectively accumulate into the tumor site. The *in vivo* tumor targetability of HA-NPs is achieved by a combination of passive and active targeting mechanisms. We found, however, that significant amounts of bare HA-NPs also accumulate in the liver. In an attempt to surmount this limitation, poly(ethylene glycol) (PEG)-conjugated HA nanoparticles (P-HA-NPs) were recently developed, and they showed improved tumor targetability *in vivo*.[39] Although PEGylation of HA-NPs slightly affects the binding affinity to the receptor on the cancer cell, PEG on the nanoparticular surface effectively reduces liver uptake and increases the circulation time in the blood, leading to selective accumulation of the nanoparticles to the tumor site.

Although several studies have demonstrated the potential of HA as the tumor-targeting moiety by chemical conjugation of HA to drugs, there have been few reports available for HA-based nanoparticles as the drug carrier.[21−23] In this study, we investigated the potential of P-HA-NPs as anticancer drug carriers. The anticancer drugs including doxorubicin (DOX) and camptothecin (CPT) were physically encapsulated into P-HA-NPs by dialysis. The drug release behaviors of P-HA-NPs were evaluated in the presence of Hyal-1, cancer cells, and tumor tissue extracts. In addition, we examined the *in vivo* biodistribution and therapeutic effects of drug-loaded P-HA-NPs following their systemic administration into tumor-bearing mice.

RESULTS AND DISCUSSION

Because P-HA-NPs are constructed using an amphiphilic HA conjugate, their hydrophobic inner cores can

serve as reservoirs for hydrophobic drugs (Figure 1a). In this study, we hypothesized that drug-loaded P-HA-NPs would effectively reach the tumor site by the EPR effect and through specific binding to CD44 on tumor cells. Once bound to CD44, the nanoparticles would be internalized by receptor-mediated endocytosis, hopefully leading to rapid degradation of the nanoparticles by Hyal-1 and the burst release of the anticancer drug for enhanced therapeutic efficacy (Figure 1b).

TABLE 1. Characteristics of Drug-Loaded P-HA-NPs

sample	loading content (wt %)	loading efficiency (%)	mean diameter (nm)
P-HA-NP			258.6 ± 7.23
DOX-P-HA-NP	32.06 ± 0.07	80.14 ± 0.09	319.6 ± 12.63
CPT-P-HA-NP	34.32 ± 0.01	85.81 ± 0.03	319.5 ± 12.79

By varying the degree of PEGylation, we previously prepared various amphiphilic HA derivatives capable of being self-assembled in an aqueous solution.[9] Among the samples tested, an HA derivative bearing five PEG molecules per 100 sugar residues of HA was selected as the drug carrier for the present study because it exhibited the highest tumor targetability *in vivo*. Owing to its amphiphilic characteristics, this HA derivative was readily self-assembled into nanoparticles (259 nm in diameter) in an aqueous condition. In cellular uptake tests, we observed that cancer cells (MDA-MB-231 and SCC7) overexpressing CD44 selectively took up P-HA-NPs *via* receptor-mediated endocytosis (Figure S1). P-HA-NPs were rapidly internalized into cancer cells, as evidenced by the presence of strong fluorescent signals observed in cells treated with Cy5.5-labeled P-HA-NPs for 10 min.

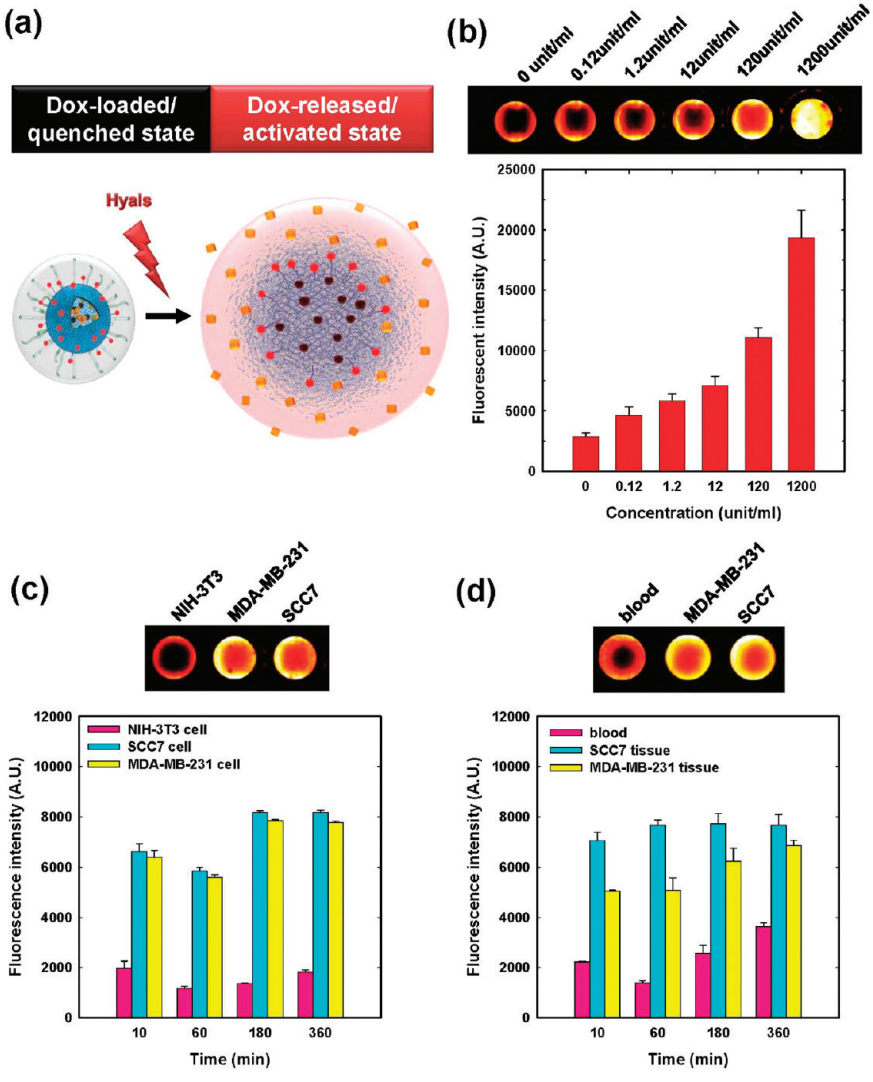

Figure 2. *In vitro* **enzyme-triggered release of DOX from P-HA-NPs. (a) Schematic diagram of DOX release from P-HA-NPs. (b) Fluorescent images and quantification of DOX-P-HA-NP after incubation with different concentrations of Hyal in acetate buffer (pH = 4.3, 37 °C) for an hour. (c, d) Fluorescent images and quantification of DOX-P-HA-NP after incubation with (c) normal cells (NIH-3T3) and cancer cells or (d) blood and extracts of tumor tissues. Error bars represent the standard deviation (*n* = 5).**

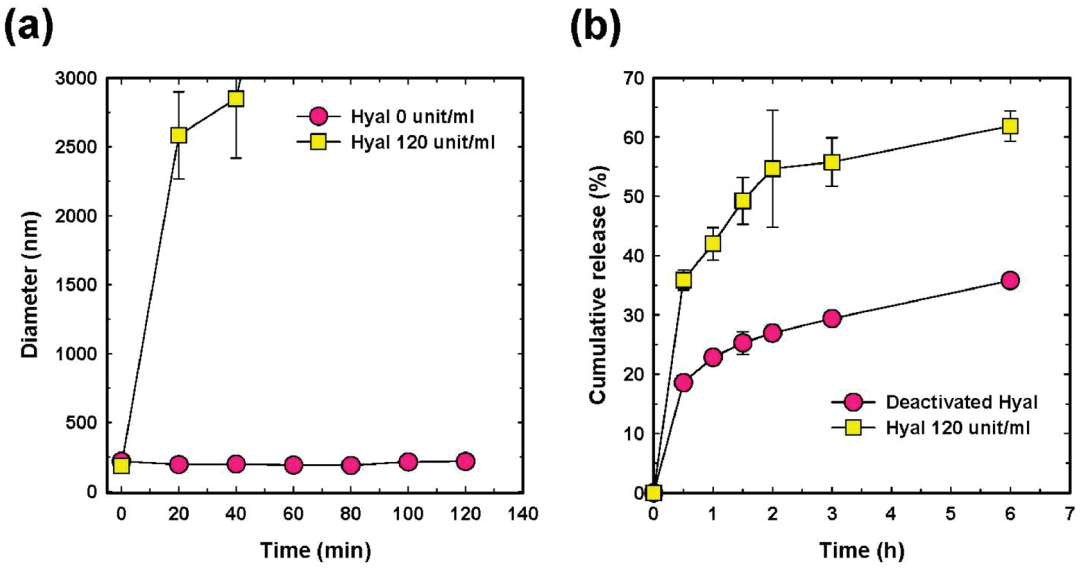

Figure 3. (a) Particle size changes of P-HA-NPs and (b) release patterns of CPT from P-HA-NPs in the presence and absence of Hyal-1. Error bars represent the standard deviation (n = 5).

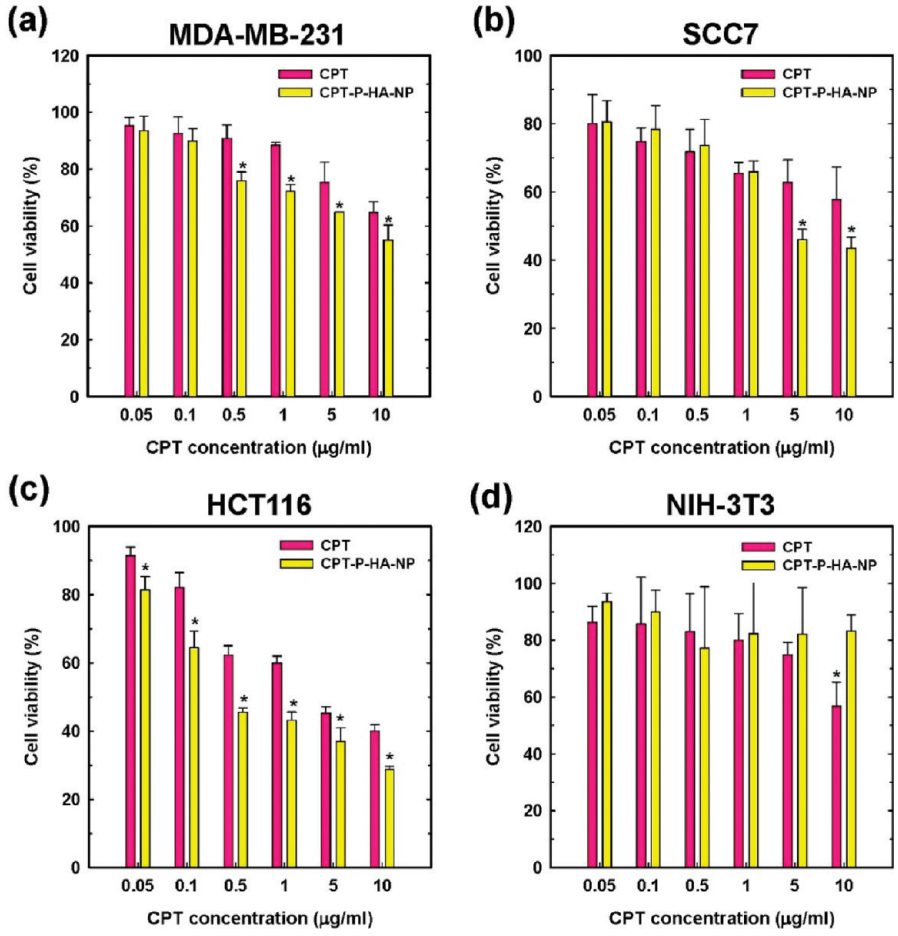

Figure 4. *In vitro* cytotoxicity of CPT and CPT-P-HA-NPs against (a) MDA-MB-231, (b) SCC7, and (c) HCT116 and normal cells ((d) NIH-3T3). Cytotoxicity of CPT-P-HA-NPs was confirmed using the MTT assay. Asterisks (*) denote statistically significant differences (*p < 0.05 compared with CPT groups) calculated by one-way ANOVA test. Error bars represent the standard deviation (n = 5).

To estimate the effect of Hyal on P-HA-NP drug release behaviors, two different anticancer drugs (DOX and CPT) were physically encapsulated into P-HA-NPs by dialysis. Table 1 details the characteristics

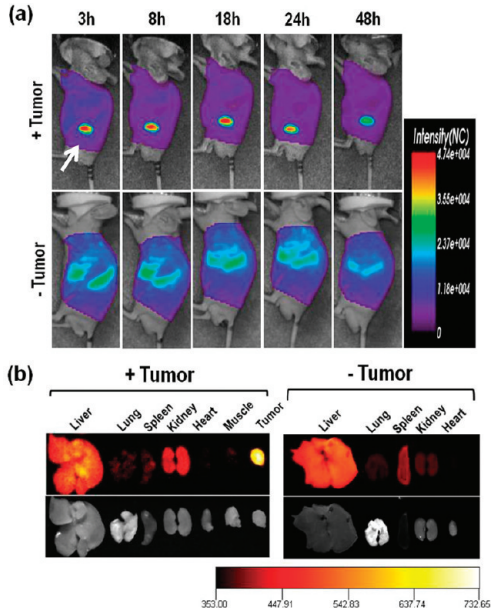

Figure 5. ***In vivo*** **noninvasive fluorescence images of CPT-P-HA-NPs in tumor-bearing mice and normal mice. (a) Whole body images of athymic nude mice with and without SCC7 tumors after intravenous injection of CPT-P-HA-NPs. The arrow indicates the tumor site. (b)** ***Ex vivo*** **fluorescence images of major organs and tumors excised at 48 h post-injection of NPs (5 mg/kg).**

of the drug-loaded P-HA-NPs. Loading efficiencies of the drugs were higher than 80%, and the mean diameter of the P-HA-NPs slightly increased following drug encapsulation (Table 1 and Figure S2).

The release behavior of DOX from P-HA-NPs was observed using fluorescence microscopy. As a hydrophobic fluorescent substance, DOX can be readily encapsulated into the hydrophobic cores of self-assembled nanoparticles in the quenched state (Figure 2a).[40] The release of DOX from nanoparticles generates a fluorescent signal, and its intensity can be measured to estimate the amount of DOX released. When DOX was loaded into P-HA-NPs, its fluorescence was highly quenched for an hour, indicating that most of DOX existed in the hydrophobic cores of the P-HA-NPs (Figure 2b). When DOX-P-HA-NPs were exposed to buffer containing Hyal-1, fluorescence intensities rose significantly due to the release of DOX from the P-HA-NPs. As Hyal-1 concentration in the buffer increased, the fluorescence intensity of DOX became stronger, suggesting that more DOX was released at higher Hyal-1 concentrations.

The release behavior of DOX from P-HA-NPs was also monitored in the presence of cancer cells or extracts of tumor tissues (Figure 2c and d). When DOX-P-HA-NPs were incubated with normal fibroblasts (NIH-3T3) or blood samples, the DOX fluorescence signals were highly quenched for over three hours. After they were incubated with cancer cells (MDA-MB-231, SCC7) or extracts of tumor tissues, however, strong fluorescence signals were detected 10 min post incubation. These results imply that P-HA-NPs rapidly release DOX in specific environments with Hyal-1.

The mean diameters of P-HA-NPs dispersed in acetate buffer without Hyal-1 exhibited no significant changes over the course of five days, suggesting a high level of stability. When incubated with Hyal-1, however, the mean diameter rapidly increased to 2584 ± 1889 nm for 10 min, implying the collapse of P-HA-NPs owing to degradation of the HA backbone by Hyal-1 (Figures 3a and S3). The release rate of CPT from P-HA-NPs was much higher in the presence of native Hyal-1 than in denatured Hyal-1 (Figure 3b). These findings are in good agreement with the fluorescence imaging of DOX-HA-NPs (Figure 2). Overall, P-HA-NPs were highly susceptible to Hyal-1, which readily destroyed their integrity and rapidly released their payloads (DOX and CPT).

In vitro cytotoxic effects of CPT-loaded NPs (CPT-P-HA-NPs) on cancer cells (MDA-MB-231, SCC7, HCT116) and normal fibroblasts (NIH-3T3) were evaluated using the MTT colorimetric assay (Figure 4). Free CPT exhibited dose-dependent cytotoxicity to all cell types tested. However, the cytotoxicity of CPT-P-HA-NPs to normal cells was significantly lower than that of free CPT and was not dependent on dose. Notably, CPT-P-HA-NPs exhibited dose-dependent cytotoxicity to cancer cells. Furthermore, high concentrations of CPT-P-HA-NPs displayed higher cytotoxicity to cancer cells than free CPT ($p < 0.05$). This difference can be explained by tumor cell-specific uptake of CPT-P-HA-NPs *via* receptor-mediated endocytosis, followed by the burst release of CPT at the intracellular level.

In vivo biodistribution and tumor targeting characteristics of NPs were monitored using a real-time near-infrared fluorescence (NIRF) imaging technique. Cy5.5-labeled CPT-P-HA-NPs were administered into the tail vein of SCC7 tumor-bearing nude mice at a dose of 5 mg/kg, and the NIRF *in vivo* images were observed as a function of time for two days. As shown in Figure 5a, considerable fluorescence signals from the CPT-P-HA-NPs were detected in the whole bodies of the mice one hour after injection, followed by a gradual decrease in the intensity of the signal as a function of time. The strongest signals were observed at the tumor sites, making the tumors easy to distinguish from normal tissues. The signal intensity at the tumor site increased for up to 18 h, after which the intensity gradually decreased for the remaining period of time. The strongest signal, however, remained at the tumor site at least for 48 h. *Ex vivo* tissue images of the organs, retrieved at 48 h post-injection, were consistent with *in vivo* imaging results (Figure 5b). These results indicate that CPT-P-HA-NPs effectively accumulated into the tumor tissue, primarily owing to their prolonged circulation in the bloodstream and specific binding to CD44 on tumor cells.

To estimate antitumor efficacy, the tumor volumes and survival rates of the tumor-bearing mice were

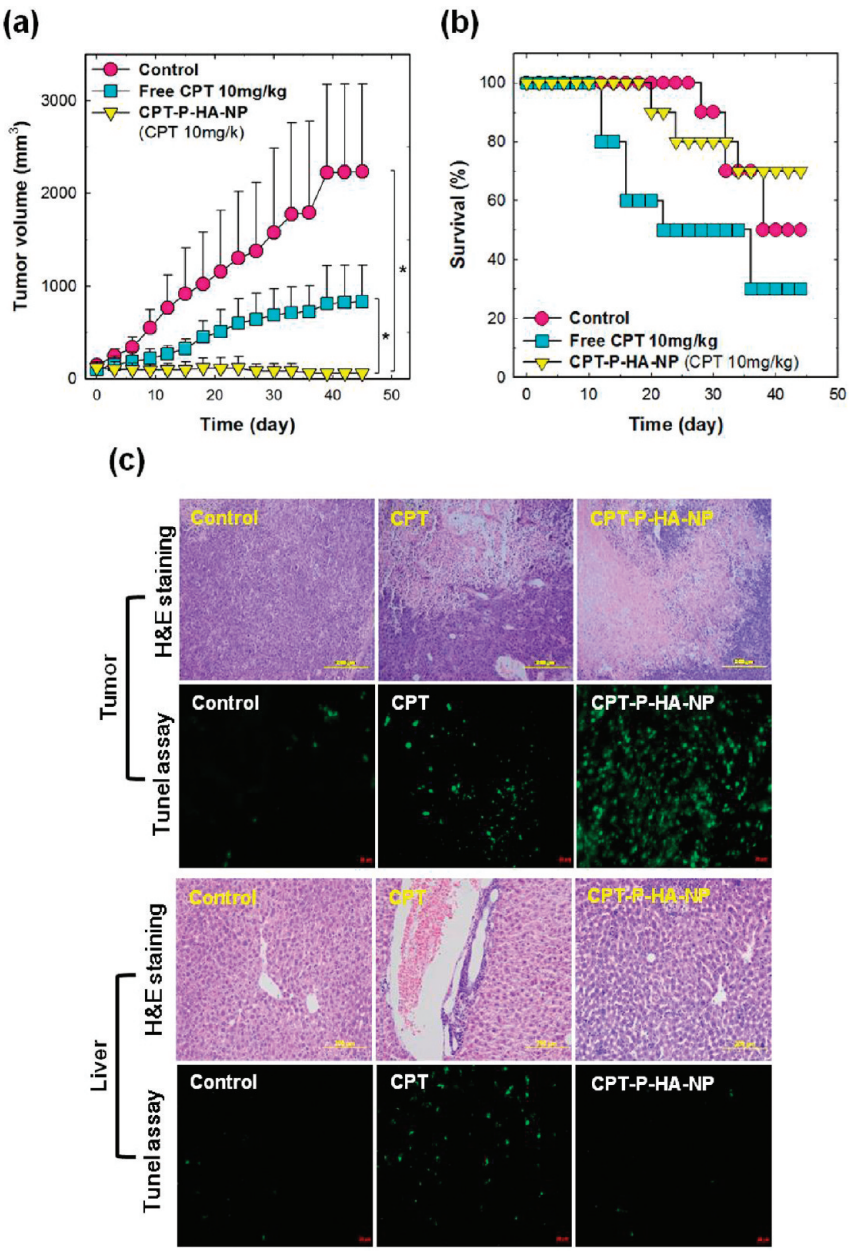

Figure 6. Antitumor efficacy of CPT-P-HA-NPs. (a) Tumor growth and (b) survival rate of MDA-MB231 human breast cancer xenografts treated with saline (○), free CPT (□), and CPT-P-HA-NPs (▽) at a CPT dose of 10 mg/kg. (c) Histological images of the tumor and liver tissues using H&E staining and the TUNEL assay. Asterisks (*) denote statistically significant differences (*$p < 0.05$) calculated by one-way ANOVA test. Error bars in (a) and (b) represent the standard deviation for 10 animals per group.

assessed after CPT-P-HA-NPs were intravenously injected at a dose of 10 mg CPT/kg into the mice once every three days (Figure 6). As expected, the control group, treated with saline, exhibited a rapid increase in tumor size as a function of time (Figure 6a). Free CPT suppressed the tumor growth for up to 10 days. Notably, no significant increase in tumor size was found for the group treated with CPT-P-HA-NPs, suggesting a high therapeutic efficacy. In terms of survival, 50% of mice treated with free CPT died within 20 days due to systemic CPT toxicity (Figure 6b). In the group treated with CPT-P-HA-NPs, however, 70% of the mice survived for 45 days. Tumor histology according to H&E staining and the TUNEL assay demonstrated that CPT-P-HA-NPs effectively delivered CPT into the tumor tissue to induce the apoptosis of tumor cells. Tumor histology according to H&E staining and the TUNEL assay demonstrated that CPT-P-HA-NPs effectively delivered CPT into the tumor tissue to induce the apoptosis of tumor cells. On the other hand, immunohistology showed that CPT-P-HA-NPs did not cause severe toxicity to the liver tissue (Figure 6c). Overall, both *in vitro* and *in vivo* results suggest that P-HA-NPs, explored in this study show promising potential as carriers of anticancer drugs.

CONCLUSION

The development of smart nanocarriers that can target tumors and release drugs in response to specific biological signals represents a valuable tactic in effective antitumor therapy. In this study, we synthesized PEGylated HA nanoparticles as potential carriers for anticancer drugs. P-HA-NPs showed tumor cell-specific uptake *in vitro via* receptor-mediated endocytosis and released the anticancer drugs in a specific environment. Most of the drugs were rapidly released from P-HA-NPs in the presence of Hyal-1, which is abundant in the intracellular compartments of cancer cells. Owing to this unique drug release behavior, CPT-P-HA-NPs showed tumor cell-specific cytotoxicity *in vitro*. In addition, CPT-P-HA-NPs demonstrated prolonged circulation in the blood and enhanced tumor-targeting characteristics *in vivo*, allowing clear visualization of the tumor site. CPT-loaded P-HA-NPs displayed excellent antitumor efficacy and a high survival rate *in vivo* compared to free CPT. P-HA-NPs may be useful carriers of hydrophobic anticancer drugs.

MATERIALS AND METHODS

Materials. Sodium hyaluronate (MW = 2.344×10^5 Da, Lifecore Biomedical, Chaska, MN, USA) was used after being dialyzed against distilled water, followed by lyophilization. 5β-Cholanic acid (CA), monomethoxy PEG-amine (PEG, MW = 5 kDa), CPT, and DOX were obtained from Sigma-Aldrich Co. (St. Louis, MO, USA). NIR dye (Cy5.5) was purchased from Amersham Biosciences (Piscataway, NJ, USA). An amphiphilic PEG-HA-CA conjugate, capable of being self-assembled into nanoparticles, was synthesized as described previously.[39] Water used for synthesis and characterization was purified by distillation, deionization, and reverse osmosis. SCC7 (squamous cell carcinoma), HCT116 (colon cancer cells), MDA-MB-231 (breast cancer cells), and NIH-3T3 (mouse embryonic fibroblast cells) were purchased from the American Type Culture Collection (Rockville, MD, USA). Hyaluronidase (Hyal) was purchased from ProSpec (NJ, USA). All other chemicals were of analytical grade and used without further purification.

Preparation and Characterization of Drug-Loaded P-HA-NPs. Drug-loaded NPs were prepared by a simple dialysis method. In brief, P-HA-NPs (20 mg) were dispersed in 20 mL of distilled water. CPT and DOX were dissolved in DMSO and DMF, respectively. The drug solution was slowly added into the P-HA-NP solution under sonication. The resulting mixture was dialyzed for one day against an excess amount of distilled water to remove unloaded drugs and organic solvent, followed by lyophilization. The particle sizes of drug-loaded nanoparticles were determined using dynamic light scattering (DLS) with a helium ion laser system (Spectra Physics Laser model 127-35, CA, USA) operated at 633 nm and 25 $\pm$ 0.1 °C. The loading contents for CPT and DOX were determined using a UV spectrometer at 365 or 490 nm, respectively.

***In Vitro* Enzyme-Triggered Drug Release of Drug-Loaded P-HA-NPs.** Hyal-triggered drug release profiles of DOX-loaded P-HA-NPs (DOX-P-HA-NPs) were monitored using a fluorescence imaging technique. Fluorescent images and quantification data of DOX-P-HA-NP solutions were obtained after the DOX-P-HA-NP solutions were incubated with different concentrations (0−1200 unit/mL) of Hyal in an acetate buffer (pH = 4.3, 37 °C) for an hour. To estimate drug release profiles of DOX-P-HA-NPs in various types of cells, we detected fluorescence intensities of DOX and attained the quantification data at predetermined time points after incubating the DOX-P-HA-NP with cell-free medium, normal cells (NIH-3T3, 1×10^6 /mL), or cancer cells (SCC7, MDA-MB-231, HCT 116 1×10^6 /mL) in 96-well flat-bottomed plates. In addition, DOX release behaviors were monitored in blood samples and tumor tissue extracts (SCC7 and MDA-MB-231) from tumor-bearing mice. To obtain the tumor tissue extracts, a suspension of cancer cells was subcutaneously injected into the dorsa of athymic nude mice (seven weeks old, 20−25 g). When the tumors reached 8 mm in diameter, we dissected and froze the tumor tissues. Frozen tissue specimens were homogenized for 30 s using a hand-held tissue homogenizer and suspended in cold buffer (50 mM Tris-HCl, pH 7.5, 0.2 M NaCl, 5 mM $CaCl_2$, 1% Triton X-100). The tissue extracts were clarified by centrifugation at 15 000 rpm for 15 min. Supernatants of tumor extracts were used for further experiments. Blood samples were harvested by heart puncture at predetermined time points, followed by centrifugation at 5000 rpm for 20 min. Supernatant fractions of blood samples were used to estimate drug release profiles in the blood.

Drug release profiles of CPT-P-HA-NPs were determined using a dialysis method in the presence of different concentrations of Hyal. In brief, lyophilized CPT-loaded NPs (1 mg) were dispersed in 1 mL of acetate buffer (pH = 4.3, 37 °C) containing different concentrations of Hyal (0 unit/mL, 24 unit/mL, and 120 units/mL). The dispersed CPT-loaded P-HA-NPs were transferred to cellulose ester dialysis tubes (molecular weight cutoff = 12 000−14 000; Spectrum) immersed in 30 mL of acetate buffer (pH = 4.3, 37 °C) and gently shaken at 37 °C in a water bath at 100 rpm. The medium was replaced with fresh medium at predetermined time points. The amount of CPT released was determined by UV spectrometry at 365 nm.

***In Vitro* Cytotoxicity of CPT-Loaded P-HA-NPs.** The cytotoxic effects of CPT and CPT-P-HA-NPs were evaluated using the MTT assay. Cells were seeded at a density of 1×10^4 cells/well in 96-well flat-bottomed plates and incubated for 24 h. Cells were washed twice with PBS and incubated in the culture medium with various concentrations of CPT and CPT-loaded NPs for 24 h at 37 °C. Cell viability was evaluated by the MTT colorimetric procedure.

***In Vivo* Real-Time Biodistribution of CPT-P-HA-NPs.** Tumor-bearing mice were prepared by injecting a suspension of 1×10^7 SCC7 cells in physiological saline (100 μL) into the subcutaneous dorsa of athymic nude mice (seven weeks old, 20−25 g). After 14 days of subcutaneous inoculation, Cy5.5-labeled CPT-P-HA-NPs were injected into the tail veins of the mice at a dose of 5 mg/kg to image their biodistribution and tumor accumulation profiles using the eXplore Optix system (ART Advanced Research Technologies Inc., Montreal, QC, Canada). At 48 h after injection, mouse organs and tumors were removed and fluorescence signals for NPs in dissected organs and tumor were detected using a Kodak imaging box (New Haven, CT, USA). For the eXplore Optix system, laser power and count time settings were optimized at 3 μW and 0.3 s per point. Excitation and emission spots were raster-scanned in 1 mm steps over the selected region of interest. A 670 nm-pulsed laser diode was used to excite the Cy5.5 molecules. The NIR fluorescence emission at 700 nm was collected and detected through a fast photomultiplier tube (Hammamatsu, Japan) and a time-correlated single photon counting system (Becker and Hickl GmbH, Berlin, Germany), respectively.

***In Vivo* Antitumor Efficacy of CPT-P-HA-NPs.** To evaluate the antitumor efficacy of CPT-P-HA-NPs, MDA-MB231 tumor-bearing mice were prepared as follows. A suspension of 1×10^7 MDA-MB231 human breast cancer cells in physiological saline (100 μL) was subcutaneously injected into the dorsa of athymic nude mice (7 weeks old, 20−25 g). Mice were divided into three groups: (i) normal saline (the control group), (ii) free CPT at 10 mg/kg, and (iii) CPT-P-HA-NPs at 10 mg CPT/kg. When tumors

reached 8 mm in diameter, each treatment was injected once every three days. The survival rates of the mice were recorded, and tumor volumes were calculated as $a \times b^2/2$, where a was the largest and b the smallest diameter. Histological changes and apoptotic cells in tumor tissues were evaluated using hematoxylin and eosin (H&E) staining and the terminal deoxynucleotidyl transferase-mediated nick end labeling (TUNEL) assay.

Statistical Analysis. The statistical significance of differences ($p < 0.05$) between groups tested was determined using one-way ANOVA.

Acknowledgment. This research was financially supported by the Korea Healthcare Technology R&D Project (A101706-1001-0000200) and the Korea Health 21 R&D Project (A062254) of MW, the Converging Research Program (20090081876) and the Basic Science Research Program (20100027955) of MEST, the Regional Technology Innovation Program (RT-104-01-01) of MKE, and BioImaging Research Center at GIST, Republic of Korea.

Supporting Information Available: Cellular uptake behavior, particle size distribution, and TEM image of nanoparticles. This information is available free of charge *via* the Internet at http://pubs.acs.org.

REFERENCES AND NOTES

1. Duncan, R. The Dawning Era of Polymer Therapeutics. *Nat. Rev. Drug Discovery* **2003**, *2*, 347–360.
2. Ferrari, M. Cancer Nanotechnology: Opportunities and Challenges. *Nat. Rev. Cancer* **2005**, *5*, 161–171.
3. Peer, D.; Karp, J. M.; Hong, S.; Farokhzad, O. C.; Margalit, R.; Langer, R. Nanocarriers as an Emerging Platform for Cancer Therapy. *Nat. Nanotechnol.* **2007**, *2*, 751–760.
4. Farokhzad, O. C.; Langer, R. Nanomedicine: Developing Smarter Therapeutic and Diagnostic Modalities. *Adv. Drug Delivery Rev.* **2006**, *58*, 1456–1459.
5. Kim, K.; Kim, J. H.; Park, H.; Kim, Y. S.; Park, K.; Nam, H.; Lee, S.; Park, J. H.; Park, R. W.; Kim, I. S.; *et al*. Tumor-Homing Multifunctional Nanoparticles for Cancer Theragnosis: Simultaneous Diagnosis, Drug Delivery, and Therapeutic Monitoring. *J. Controlled Release* **2010**, *146*, 219–227.
6. Kim, J. H.; Kim, Y. S.; Park, K.; Lee, S.; Nam, H. Y.; Min, K. H.; Jo, H. G.; Park, J. H.; Choi, K.; Jeong, S. Y.; *et al*. Antitumor Efficacy of Cisplatin-Loaded Glycol Chitosan Nanoparticles in Tumor-Bearing Mice. *J. Controlled Release* **2008**, *127*, 41–49.
7. Farokhzad, O. C.; Langer, R. Impact of Nanotechnology on Drug Delivery. *ACS Nano* **2009**, *3*, 16–20.
8. Wang, X.; Li, J.; Wang, Y.; Cho, K. J.; Kim, G.; Gjyrezi, A.; Koenig, L.; Giannakakou, P.; Shin, H. J.; Tighiouart, M.; *et al*. Hft-T, A Targeting Nanoparticle Enhances Specific Delivery of Paclitaxel to Folate Receptor-Positive Tumors. *ACS Nano* **2009**, *3*, 3165–3174.
9. Choi, K. Y.; Chung, H.; Min, K. H.; Yoon, H. Y.; Kim, K.; Park, J. H.; Kwon, I. C.; Jeong, S. Y. Self-Assembled Hyaluronic Acid Nanoparticles for Active Tumor Targeting. *Biomaterials* **2010**, *31*, 106–114.
10. Bae, Y.; Fukushima, S.; Harada, A.; Kataoka, K. Design of Environment-Sensitive Supramolecular Assemblies for Intracellular Drug Delivery: Polymeric Micelles That Are Responsive to Intracellular Ph Change 13. *Angew. Chem., Int. Ed.* **2003**, *42*, 4640–4643.
11. Ko, J.; Park, K.; Kim, Y.-S.; Kim, M. S.; Han, J. K.; Kim, K.; Park, R.-W.; Kim, I.-S.; Song, H. K.; Lee, D. S.; *et al*. Tumoral Acidic Extracellular pH Targeting of pH-Responsive Mpeg-Poly ([Beta]-Amino Ester) Block Copolymer Micelles for Cancer Therapy. *J. Controlled Release* **2007**, *123*, 109–115.
12. Lee, E. S.; Gao, Z.; Bae, Y. H. Recent Progress in Tumor pH Targeting Nanotechnology. *J. Controlled Release* **2008**, *132*, 164–170.
13. Lee, Y.; Fukushima, S.; Bae, Y.; Hiki, S.; Ishii, T.; Kataoka, K. A Protein Nanocarrier from Charge-Conversion Polymer in Response to Endosomal pH. *J. Am. Chem. Soc.* **2007**, *129*, 5362–5363.
14. Lee, S. M.; Ahn, R. W.; Chen, F.; Fought, A. J.; O'Halloran, T. V.; Cryns, V. L.; Nguyen, S. T. Biological Evaluation of pH-Responsive Polymer-Caged Nanobins for Breast Cancer Therapy. *ACS Nano* **2010**, *4*, 4971–4978.
15. Koo, A. N.; Lee, H. J.; Kim, S. E.; Chang, J. H.; Park, C.; Kim, C.; Park, J. H.; Lee, S. C. Disulfide-Cross-Linked Peg-Poly-(Amino Acid)s Copolymer Micelles for Glutathione-Mediated Intracellular Drug Delivery. *Chem. Commun.* **2008**, 6570–6572.
16. Miyata, K.; Kakizawa, Y.; Nishiyama, N.; Harada, A.; Yamasaki, Y.; Koyama, H.; Kataoka, K. Block Catiomer Polyplexes with Regulated Densities of Charge and Disulfide Cross-Linking Directed to Enhance Gene Expression. *J. Am. Chem. Soc.* **2004**, *126*, 2355–2361.
17. Haba, K.; Popkov, M.; Shamis, M.; Lerner, R. A.; C., F. B., III; Shabat, D. Single-Triggered Trimeric Prodrugs 13. *Angew. Chem., Int. Ed.* **2005**, *44*, 716–720.
18. Biswas, A.; Joo, K. I.; Liu, J.; Zhao, M.; Fan, G.; Wang, P.; Gu, Z.; Tang, Y. Endoprotease-Mediated Intracellular Protein Delivery Using Nanocapsules. *ACS Nano* **2011**, *5*, 1385–1394.
19. Lapcik, L. J.; Lapcik, L.; De Smedt, S.; Demeester, J.; Chabrecek, P. Hyaluronan: Preparation, Structure, Properties, and Applications. *Chem. Rev.* **1998**, *98*, 2663–2684.
20. Toole, B. P. Hyaluronan: From Extracellular Glue to Pericellular Cue. *Nat. Rev. Cancer* **2004**, *4*, 528–539.
21. Eliaz, R. E.; Szoka, F. C., Jr. Liposome-Encapsulated Doxorubicin Targeted to Cd44: A Strategy to Kill Cd44-Overexpressing Tumor Cells. *Cancer Res.* **2001**, *61*, 2592–2601.
22. Platt, V. M.; Szoka, F. C., Jr. Anticancer Therapeutics: Targeting Macromolecules and Nanocarriers to Hyaluronan or Cd44, a Hyaluronan Receptor. *Mol. Pharm.* **2008**, *5*, 474–486.
23. Auzenne, E.; Ghosh, S. C.; Khodadadian, M.; Rivera, B.; Farquhar, D.; Price, R. E.; Ravoori, M.; Kundra, V.; Freedman, R. S.; Klostergaard, J. Hyaluronic Acid-Paclitaxel: Antitumor Efficacy against Cd44(+) Human Ovarian Carcinoma Xenografts. *Neoplasia* **2007**, *9*, 479–486.
24. Stern, R.; Jedrzejas, M. J. Hyaluronidases: Their Genomics, Structures, and Mechanisms of Action. *Chem. Rev.* **2006**, *106*, 818–839.
25. Lokeshwar, V. B.; Lokeshwar, B. L.; Pham, H. T.; Block, N. L. Association of Elevated Levels of Hyaluronidase, a Matrix-Degrading Enzyme, with Prostate Cancer Progression. *Cancer Res.* **1996**, *56*, 651–657.
26. Lokeshwar, V. B.; Cerwinka, W. H.; Isoyama, T.; Lokeshwar, B. L. Hyal1 Hyaluronidase in Prostate Cancer: A Tumor Promoter and Suppressor. *Cancer Res.* **2005**, *65*, 7782–7789.
27. Chao, K. L.; Muthukumar, L.; Herzberg, O. Structure of Human Hyaluronidase-1, a Hyaluronan Hydrolyzing Enzyme Involved in Tumor Growth and Angiogenesis. *Biochemistry* **2007**, *46*, 6911–6920.
28. Pham, H. T.; Block, N. L.; Lokeshwar, V. B. Tumor-Derived Hyaluronidase: A Diagnostic Urine Marker for High-Grade Bladder Cancer. *Cancer Res.* **1997**, *57*, 778–783.
29. Franzmann, E. J.; Schroeder, G. L.; Goodwin, W. J.; Weed, D. T.; Fisher, P.; Lokeshwar, V. B. Expression of Tumor Markers Hyaluronic Acid and Hyaluronidase (Hyal1) in Head and Neck Tumors. *Int. J. Cancer* **2003**, *106*, 438–445.
30. Liu, D.; Pearlman, E.; Diaconu, E.; Guo, K.; Mori, H.; Haqqi, T.; Markowitz, S.; Willson, J.; Sy, M. S. Expression of Hyaluronidase by Tumor Cells Induces Angiogenesis in Vivo. *Proc. Natl. Acad. Sci. U. S. A.* **1996**, *93*, 7832–7837.
31. Delpech, B.; Laquerriere, A.; Maingonnat, C.; Bertrand, P.; Freger, P. Hyaluronidase Is More Elevated in Human Brain Metastases Than in Primary Brain Tumours. *Anticancer Res.* **2002**, *22*, 2423–2427.
32. Bertrand, P.; Girard, N.; Duval, C.; d'Anjou, J. L.; Chauzy, C.; Ménard, J.-F. I.; Delpech, B. Increased Hyaluronidase Levels in Breast Tumor Metastases. *Int. J. Cancer* **1997**, *73*, 327–331.
33. Bourguignon, L. Y.; Singleton, P. A.; Diedrich, F.; Stern, R.; Gilad, E. Cd44 Interaction with Na^+-H^+ Exchanger (Nhe1) Creates Acidic Microenvironments Leading to Hyaluronidase-2 and Cathepsin B Activation and Breast Tumor Cell Invasion. *J. Biol. Chem.* **2004**, *279*, 26991–27007.
34. Stern, R. Hyaluronidases in Cancer Biology. *Semin. Cancer Biol.* **2008**, *18*, 275–280.

35. Kumar, S.; West, D. C.; Ponting, J. M.; Gattamaneni, H. R. Sera of Children with Renal Tumours Contain Low-Molecular-Mass Hyaluronic Acid. *Int. J. Cancer* **1989**, *44*, 445–448.
36. Itano, N. Simple Primary Structure, Complex Turnover Regulation and Multiple Roles of Hyaluronan. *J. Biochem.* **2008**, *144*, 131–137.
37. Coradini, D.; Perbellini, A. Hyaluronan: A Suitable Carrier for an Histone Deacetylase Inhibitor in the Treatment of Human Solid Tumors. *Cancer Ther.* **2004**, *2*, 201–216.
38. Choi, K. Y.; Min, K. H.; Na, J. H.; Choi, K.; Kim, K.; Park, J. H.; Kwon, I. C.; Jeong, S. Y. Self-Assembled Hyaluronic Acid Nanoparticles as a Potential Drug Carrier for Cancer Therapy: Synthesis, Characterization, and in Vivo Biodistribution. *J. Mater. Chem.* **2009**, *19*, 4102–4107.
39. Choi, K. Y.; Min, K. H.; Yoon, H. Y.; Kim, K.; Park, J. H.; Kwon, I. C.; Choi, K.; Jeong, S. Y. Pegylation of Hyaluronic Acid Nanoparticles Improves Tumor Targetability in Vivo. *Biomaterials* **2011**, *32*, 1880–1889.
40. Kwon, G. S.; Naito, M.; Yokoyama, M.; Okano, T.; Sakurai, Y.; Kataoka, K. Physical Entrapment of Adriamycin in Ab Block Copolymer Micelles. *Pharm. Res.* **1995**, *12*, 192–195.